International Journal of Environmental Sciences
ISSN: 2229-7359
Vol. 11 No. 24s, 2025
https://www.theaspd.com/ijes.php

Development And Evaluation Of Baricitinib -Gel Loaded Transdermal Patches For Treatment In Rheumatoid Arthritis

Mr. Bharat V. Jadhav[1]*, Dr. Sanjay Bhawar.[2]
[1]Research Scholar, Bhagwant University, Ajmer, India
[2]Professor and Principal, Pravara Rural College of Pharmacy, Loni, Maharashtra, India

Abstract

Objectives: *The study aimed to develop and optimize a baricitinib-loaded transdermal gel-patch system for enhanced delivery in rheumatoid arthritis management, improving drug release, skin permeability, and therapeutic efficacy.*

Methods: *A transdermal gel was formulated using Carbopol 940P and propylene glycol, and optimized using a 3^2 full factorial design. Evaluations included physicochemical characterization, ex vivo permeation, in vitro drug release, FTIR and DSC compatibility studies, and in vivo anti-arthritic activity in a CFA-induced rat model. The optimized gel was incorporated into a patch system and assessed for mechanical and stability parameters.*

Results: *The optimized formulation (F9) exhibited desirable viscosity (3789 ± 165 cP), spreadability (1.6 ± 0.09 cm), drug content (98.8 ± 1.1%), and gel strength (312 ± 16 g). Batch F9 demonstrated the highest sustained drug release (94.8 ± 3.0% at 12 h) (Figure 4). The selected optimized patch (GT3) showed a steady-state flux of 21.5 ± 1.2 μg/cm²/h and 66.9 ± 2.8% drug release at 12 h (Figure 6), with improved folding endurance and adhesion strength (445 ± 25 and 0.94 ± 0.06 N/cm², respectively). In vivo studies confirmed superior arthritis score reduction (7.2 ± 1.2), 60.8% paw volume inhibition, improved hematological and cytokine profiles, and weight recovery. GT3 remained stable over 6 months under accelerated conditions (Table 12).*

Conclusion: *The optimized baricitinib-loaded gel patch (GT3) demonstrated sustained release, enhanced permeability, and effective anti-arthritic activity, indicating strong potential for clinical translation in chronic inflammatory conditions like rheumatoid arthritis.*

Keywords: *Baricitinib, transdermal patch, factorial design, rheumatoid arthritis, in vivo evaluation, sustained release.*

INTRODUCTION

Rheumatoid arthritis (RA) is a chronic, systemic autoimmune disease affecting approximately 0.5–1% of the global population, with higher prevalence in women and older adults [1]. It causes progressive joint destruction, disability, and a significant reduction in quality of life [2]. According to the World Health Organization, over 18 million people are currently living with RA worldwide, with the number expected to rise due to aging populations and lifestyle factors [3]. RA imposes a substantial economic burden, with direct healthcare costs and indirect losses due to reduced productivity reaching billions annually. Traditional therapies, including non-steroidal anti-inflammatory drugs (NSAIDs) and disease-modifying anti-rheumatic drugs (DMARDs), often exhibit limited efficacy and systemic side effects [4]. Biologics, while effective, are costly and require parenteral administration, limiting patient compliance. Moreover, oral administration of drugs like baricitinib is often associated with first-pass metabolism and gastrointestinal complications. Hence, there is a growing need for alternative drug delivery systems that enhance bioavailability, reduce systemic toxicity, and improve therapeutic outcomes [5].

Baricitinib, a selective Janus kinase (JAK1/JAK2) inhibitor, has emerged as a promising oral DMARD approved for moderate-to-severe RA [6]. Chemically, it is a pyrazolopyrimidine derivative with favorable molecular properties, including moderate lipophilicity and low molecular weight (~371.4 g/mol), making it suitable for transdermal absorption. Its mechanism involves inhibition of JAK-mediated cytokine signaling, particularly interleukin-6 and interferon-gamma, crucial in RA pathogenesis [7]. Clinical trials have demonstrated its ability to reduce inflammation, joint damage, and disease progression with a favorable safety profile. However, oral baricitinib therapy may cause systemic adverse effects such as infections and thrombosis [8]. Recent preclinical and clinical studies have explored its repurposing in other inflammatory conditions and viral infections due to its immunomodulatory potential [9]. Despite its therapeutic promise, there remains a need to refine its delivery to enhance site-specific action, reduce dose frequency, and improve patient adherence highlighting the need for innovative delivery systems [10].

Transdermal drug delivery systems (TDDS) offer a non-invasive, controlled-release platform capable of bypassing hepatic first-pass metabolism and maintaining steady plasma drug levels. In the context of RA, transdermal patches provide targeted delivery, reduce systemic toxicity, and enhance patient compliance [11]. The present study proposes a novel baricitinib-loaded gel-based transdermal patch incorporating a biocompatible polymer matrix designed to optimize drug diffusion through the skin. The gel formulation ensures enhanced permeation, moisture retention, and extended residence time at the site of application [12]. Compared to oral or injectable formulations, transdermal systems offer significant benefits, including minimal dosing frequency and sustained therapeutic levels [13]. Advances in patch technology, such as hydrogel matrices and permeation enhancers, have demonstrated promise in improving skin permeability for drugs with moderate molecular weight. Previous reports have validated the feasibility of delivering JAK inhibitors transdermally using suitable carriers [14]. Thus, developing a gel-loaded patch formulation of baricitinib aligns with current trends in personalized, non-invasive RA therapy, offering a superior alternative to conventional approaches [15].

The present study aims to develop and evaluate a baricitinib-loaded gel-based transdermal patch for effective RA management. Specific objectives include formulation optimization, physicochemical characterization, in vitro release, ex vivo permeation, and skin irritation studies. This research addresses critical limitations in oral therapy and proposes an innovative, patient-friendly delivery platform with potential for clinical translation.

MATERIALS AND METHOD

MATERIALS

Baricitinib (analytical grade, MW: 371.42 g/mol) was procured from Sciquaint Innovations (Pune, India). Carbopol 940P (analytical grade, viscosity: 40,000–60,000 cps) was purchased from Lubrizol Advanced Materials (Mumbai, India). Propylene glycol (USP grade, ≥99.5% purity) was obtained from Loba Chemie Pvt. Ltd. (Mumbai, India). Methanol and ethanol (HPLC grade, ≥99.9% purity) were sourced from Merck Life Science Pvt. Ltd. (Mumbai, India). DMSO (analytical grade, ≥99.9% purity) was obtained from Sigma-Aldrich (Bangalore, India). Phosphate buffer components (analytical grade) were procured from Qualigens Fine Chemicals (Mumbai, India). All other chemicals and reagents used in this study were of analytical grade and used as received without further purification.

METHODS

Calibration curve determination

A calibration curve for Baricitinib was developed using a UV-Visible spectrophotometer (Shimadzu UV-1900, Kyoto, Japan) for accurate quantitative analysis. A stock solution of 100 µg/mL was prepared by dissolving 10 mg of Baricitinib in methanol and diluting to 100 mL with the same solvent. From this, working solutions in the range of 5 to 30 µg/mL were prepared by serial dilution with methanol. Absorbance of each solution was measured at 252 nm against methanol as blank at 25 ± 2 °C. All measurements were performed in triplicate (n = 3). A calibration curve was plotted with concentration on the X-axis and absorbance on the Y-axis. The linear regression equation and correlation coefficient ($R^2 > 0.999$) confirmed excellent linearity. The method adhered to ICH Q2(R1) guidelines and was found suitable for Baricitinib quantification in analytical procedures [16].

Solubility study

The solubility of Baricitinib was determined in various solvents methanol, ethanol, distilled water, phosphate buffer pH 6.8, and dimethyl sulfoxide (DMSO) using the solvent saturation method. Excess amount of Baricitinib was added to 10 mL of each solvent in separate glass vials, which were then sealed and stirred using a magnetic stirrer (Remi Equipments, India) at 25 ± 2 °C for 24 hours to attain equilibrium. After equilibration, the mixtures were filtered through 0.45 µm membrane filters to remove undissolved drug. The filtrates were appropriately diluted with their respective solvents, and the drug concentration was measured using a UV-Visible spectrophotometer (Shimadzu UV-1900, Kyoto, Japan) at 252 nm. All experiments were performed in triplicate (n = 3). The solubility values were calculated in mg/mL, allowing comparative evaluation of Baricitinib solubility across different solvents for use in formulation selection [17].

Differential scanning calorimetry

Differential Scanning Calorimetry (DSC) was performed to evaluate the thermal behavior and compatibility of Baricitinib with excipients. Samples of pure drug, individual excipients (HPMC K15M, Eudragit RL100, PEG 400), and their physical mixture were analyzed using a DSC instrument (DSC 4000, PerkinElmer, USA). Accurately weighed samples (2–5 mg) were sealed in aluminum pans and

heated from 30 °C to 300 °C at a rate of 10 °C/min under nitrogen flow (40 mL/min). An empty aluminum pan served as the reference. Thermograms were examined for melting point, peak shifts, or disappearance to assess drug–excipient interactions. All tests were performed in triplicate (n = 3) for consistency [18].

Fourier Transform Infrared (FTIR)

Fourier Transform Infrared (FTIR) spectroscopy was carried out to evaluate possible interactions between Baricitinib and formulation excipients. FTIR spectra of pure drug, individual excipients (HPMC K15M, Eudragit RL100, PEG 400), and their physical mixture were recorded using an FTIR spectrometer (Alpha II, Bruker, Germany) equipped with an ATR (attenuated total reflectance) accessory. About 1–2 mg of each sample was placed directly on the crystal surface, and spectra were scanned over a range of 4000–400 cm^{-1} at a resolution of 4 cm^{-1} with 32 scans per sample. Characteristic peaks of functional groups were compared across the samples to detect any significant shifts, disappearance, or new peak formation indicating potential interactions. All analyses were performed in triplicate (n = 3) to ensure reproducibility [19].

Experimental Design for Formulations (3^2 Factorial Design)

A 3^2 full factorial design was employed to optimize gel-loaded transdermal patch formulation and study effect of independent variables on dependent variables. Two independent variables were selected: X_1 = Concentration of Carbopol 940P (0.5%, 1.0%, 1.5% w/w) and X_2 = Concentration of Propylene Glycol (10%, 15%, 20% w/w). Dependent variables (responses) were: Y_1 = Cumulative drug release at 8 hours (%), Y_2 = Flux (μg/cm^2/h), Y_3 = Gel viscosity (cP), and Y_4 = Patch adhesion strength (N/cm^2).

$Y = b_0 + b_1X_1 + b_2X_2 + b_{12}X_1X_2 + b_{11}X_1^2 + b_{22}X_2^2$

Where Y = response, b_0 = intercept, b_1 and b_2 = main effects, b_{12} = interaction effect, b_{11} and b_{22} = quadratic effects [20,21].

Table 1: Independent Variables and Their Levels

Variables	Low Level (-1)	Medium Level (0)	High Level (+1)
X_1: Carbopol 940P (% w/w)	0.5	1.0	1.5
X_2: Propylene Glycol (% w/w)	10	15	20
Dependent Variables			**Goals**
Gel viscosity (cP)			Optimize
Cumulative drug release at 8h (%)			Maximize

Preparation of Baricitinib Gel

A gel containing baricitinib and novel permeation enhancers was prepared for transdermal patch application. Baricitinib (20 mg) was dissolved in methanol (2 mL) using an ultrasonic bath (Lab India, Mumbai, India) for 10 minutes. Oleyl pyrrolidone (5.0 mg) and dodecyl prolinate (2.5 mg) were added sequentially with continuous stirring. Separately, Carbopol 940P (1.0% w/w) was dispersed in distilled water using a magnetic stirrer (Remi Motors, Mumbai, India) at 500 rpm for 30 minutes. A solution of N-methyl pyrrolidone (0.5% w/w) and niacinamide (1.0 mg) was added to the polymer dispersion. The drug-enhancer mixture was then slowly incorporated into the gel base under constant stirring, followed by addition of propylene glycol (5% w/v) as a co-enhancer. The pH was adjusted to 6.5–7.0 using 0.2 mL triethanolamine with stirring at 300 rpm for 15 minutes. The final volume was made up to 10 mL with distilled water, and the gel was allowed to stand for 2 hours to remove air bubbles. Formulations were prepared in triplicate (n=3) [22].

Table 2: Formulation Composition for 3^2 Factorial Design with Novel Permeation Enhancers

Component	F1	F2	F3	F4	F5	F6	F7	F8	F9
Baricitinib (mg)	20	20	20	20	20	20	20	20	20
Carbopol 940P (% w/w)	0.5	0.5	0.5	1.0	1.0	1.0	1.5	1.5	1.5
Propylene Glycol (% w/w)	10	15	20	10	15	20	10	15	20
Oleyl Pyrrolidone (mg)	5.0	5.0	5.0	5.0	5.0	5.0	5.0	5.0	5.0
Dodecyl Prolinate (mg)	2.5	2.5	2.5	2.5	2.5	2.5	2.5	2.5	2.5
N-methyl Pyrrolidone (% w/w)	0.5	0.5	0.5	0.5	0.5	0.5	0.5	0.5	0.5
Niacinamide (mg)	1.0	1.0	1.0	1.0	1.0	1.0	1.0	1.0	1.0

Triethanolamine (mL)	0.2	0.2	0.2	0.2	0.2	0.2	0.2	0.2	0.2
Methanol (mL)	2	2	2	2	2	2	2	2	2
Distilled Water (mL)	q.s. to 10	q.s. to 10	q.s. to 10	q.s. to 10	q.s. to 10	q.s. to 10	q.s. to 10	q.s. to 10	q.s. to 10

Preparation of Gel-Loaded Transdermal Patches

Reservoir-type gel-loaded transdermal patches were prepared using the solvent casting method. HPMC E5 (3% w/v) was dissolved in distilled water with gentle heating at 60 °C and stirred for 30 minutes (Remi Motors, Mumbai, India). The solution was cast onto aluminum foil-lined petri dishes (9 cm) and dried at 40 °C for 6 hours (Lab India, Mumbai, India). Circular reservoirs (2 cm) were cut at the center, and 0.5 mL of optimized baricitinib gel (1 mg drug) was loaded. A 4% w/v cellulose acetate solution in acetone-water (8:2) was cast as a rate-controlling membrane. After drying, edges were sealed at 65 °C for 45 seconds using an impulse sealer. Medical-grade acrylic adhesive was applied around the border, leaving a 1 mm margin. Patches were cut to 4 cm^2 using a die cutter and stored in aluminum pouches with desiccant at 25 ± 2 °C. Each batch was prepared in triplicate (n=3) and tested as per pharmacopeial standards [23].

Table 3: Formulation Composition of Gel-Loaded Transdermal Patch Batches

Ingredient	**GT1**	**GT2**	**GT3**	**GT4**
Optimized Baricitinib Gel (mL)	0.5	0.5	0.5	0.5
HPMC E5 for Backing (% w/v)	3.0	3.5	4.0	4.5
Cellulose Acetate for Rate Control (% w/v)	3.0	3.5	4.0	4.5
Acetone (mL)	8.0	8.0	8.0	8.0
Distilled Water (mL)	2.0	2.0	2.0	2.0
Acrylic Adhesive (mg)	50	60	70	80
Polyethylene Glycol 400 (Plasticizer) (µL)	20	25	30	35

Characterization of Baricitinib Gel

pH Measurement

The pH of the prepared baricitinib gels was measured to ensure skin compatibility and formulation stability. A digital pH meter (pH-700, Eutech Instruments, Mumbai, India) was calibrated with standard buffers (pH 4.0, 7.0, and 9.2) at 25 ± 2 °C. One gram of gel was dispersed in 10 mL of distilled water and stirred at 100 rpm for 10 minutes. The electrode was immersed in the dispersion, and pH was recorded after 2 minutes of stabilization. Each sample was tested in triplicate (n=3), and results were reported as mean ± SD. Data were statistically analyzed using one-way ANOVA followed by Tukey's post hoc test [24].

Viscosity Determination

The viscosity of baricitinib gels was evaluated to determine flow behavior and suitability for patch loading using a Brookfield DV-II+ Pro viscometer (Brookfield Engineering Laboratories, Mumbai, India) fitted with spindle SC4-21. Gel samples (50 mL) were maintained at 25 ± 1 °C using a circulating water bath and tested over shear rates ranging from 0.1 to 100 rpm, with a 30-second interval between readings. Apparent viscosity (cP) was recorded at 10 rpm, and rheograms were constructed by plotting viscosity against shear rate. Flow index (n) and consistency index (K) were calculated using the power law equation: $\tau = K \times \gamma^n$. Measurements were performed in triplicate (n = 3), and results were reported as mean ± SD [25].

Spreadability Study

Spreadability was assessed to evaluate gel application efficiency by placing 0.5 g of gel between two glass slides (7.5 × 2.5 cm) and allowing it to spread under its own weight for 1 minute, followed by placement of a 1000 g weight for 5 minutes. The diameter of the spread area was measured in four directions using vernier calipers and averaged. Spreadability (S) was calculated using the formula $S = d^2 \times \pi/4$, where d is the average diameter. Tests were conducted at 25 ± 2 °C in triplicate (n = 3), and values were expressed as mean ± SD. Statistical significance was determined using Student's *t*-test [26].

Drug Content Determination

aricitinib content in gels was determined to ensure uniform drug loading. Gel equivalent to 10 mg drug was mixed with 50 mL phosphate buffer (pH 7.4) and sonicated for 30 minutes at 40 °C (Lab India,

Mumbai, India). After cooling, the volume was made up to 100 mL, filtered through a 0.45 µm membrane (Millipore, Mumbai, India), and appropriately diluted. Absorbance was measured at 247 nm using a UV-Visible spectrophotometer (UV-2450, Shimadzu, Mumbai, India). Tests were done in triplicate (n = 3), and results were calculated using a calibration curve and expressed as % drug content ± SD [27].

Gel Strength Assessment

Gel strength was assessed to evaluate the mechanical integrity of the formulation using a texture analyzer (TA.XT plus, Stable Micro Systems, Mumbai, India) with a 5 mm cylindrical probe. Gel samples (25 g) were placed in 50 mL beakers and equilibrated at 25 ± 2 °C for 2 hours. The probe was driven at 1 mm/sec to a depth of 10 mm with a 0.5 g trigger force; pre-test and post-test speeds were set at 2 mm/sec. Maximum force (g) required for penetration was recorded as gel strength. Tests were performed in triplicate (n = 3), and results were expressed as mean ± SD. Data analysis was conducted using Exponent software and one-way ANOVA [28].

Extrudability Study

Extrudability was evaluated to assess ease of gel removal and uniform flow for patch loading. Aluminum collapsible tubes (5 mm orifice) were filled with 10 g gel and sealed. A 1 kg weight was applied for 30 seconds at 25 ± 2 °C, and the extruded gel was weighed. Extrudability was calculated as the percentage of gel extruded relative to the initial weight. The test was performed using a universal testing machine (Instron 3345, Mumbai, India) at a compression rate of 10 mm/min. Visual inspection was done for extrusion smoothness and absence of air pockets. Measurements were taken in triplicate (n = 3) and results expressed as mean ± SD. Statistical analysis was performed using one-way ANOVA followed by Tukey's test [29].

In Vitro Drug Release Study

Drug release from baricitinib gels was studied using Franz diffusion cells (diffusion area: 3.14 cm^2; receptor volume: 15 mL) with cellulose acetate membrane (MWCO 12,000–14,000 Da, pore size 0.45 µm). The membrane was pre-soaked in phosphate buffer (pH 7.4) for 30 minutes. The receptor compartment contained phosphate buffer with 20% PEG-400, maintained at 32 ± 1 °C and stirred at 100 rpm. Gel equivalent to 2 mg baricitinib was placed in the donor chamber, covered with aluminum foil. Samples (1 mL) were withdrawn at intervals up to 12 hours and replaced with fresh buffer. Absorbance was measured at 247 nm using a UV-Visible spectrophotometer, and cumulative release was calculated. Each test was done in triplicate (n = 3), and release data were fitted to zero-order, first-order, Higuchi, and Korsmeyer-Peppas models [30].

Characterization of Gel-Loaded Transdermal Patches

Physical Appearance and Visual Inspection

Gel-loaded patches were visually inspected under 1000 lux light using a 10× magnifying glass to assess color uniformity, surface smoothness, flexibility, and absence of bubbles or crystals. Backing membrane and edge seals were checked for cracks, pinholes, and leakage. Ten patches per batch (n=10) were examined, and defects were documented and classified as major or minor. Results were expressed as the percentage of defect-free patches [31].

Thickness Uniformity

Patch thickness was measured using a digital micrometer screw gauge (Mitutoyo Corporation, Mumbai, India) with 0.001 mm precision. Six points per patch (center, four corners, one random) were assessed without excess pressure. Measurements were performed on 10 patches per batch at 25 ± 2 °C and 60 ± 5% RH. Mean thickness, standard deviation, and coefficient of variation (CV) were calculated. Acceptable deviation was ±5% from the mean, and CV < 5%. Statistical comparison across batches was conducted using one-way ANOVA [32].

Weight Variation Analysis

Patches (4 cm^2) were individually weighed using an analytical balance (Sartorius BSA224S, Mumbai, India; 0.1 mg precision) to assess uniformity. Twenty patches per batch were randomly selected and weighed under controlled conditions (25 ± 2 °C, 60 ± 5% RH). Mean weight, % deviation, and coefficient of variation were calculated. According to pharmacopeial limits, no more than two patches may deviate by ±5%, and none by ±10%. Weight data also supported drug content uniformity, assuming proportional drug distribution. One-way ANOVA was used for statistical comparison [33].

Folding Endurance Test

Flexibility of patches was assessed by folding 2 × 2 cm patches repeatedly at the same point until cracking or breakage occurred. Folding was performed at 25 ± 2 °C using an automated apparatus (Lab India, Mumbai, India) at 1 fold/sec. The number of folds required for damage was recorded as folding

endurance. Ten patches per batch were tested, and results expressed as mean ± SD. Values below 200 indicated poor, while >500 denoted excellent flexibility [34].

Patch Adhesion Studies

Adhesive strength was measured using a texture analyzer (TA.XT plus, Stable Micro Systems, Mumbai, India) with a 25 mm cylindrical probe. Patches were pressed onto stainless steel plates (2 kg, 30 s) and allowed to adhere for 5 minutes at 32 ± 1 °C. The probe detached the patch vertically at 1 mm/sec. Peak force was recorded in Newtons and converted to N/cm². Tests were done in triplicate (n = 3) under 50 ± 5% RH. Minimum acceptable strength was 0.5 N/cm² and results were compared with commercial patches [35].

Drug Content Uniformity

Drug content uniformity was evaluated by cutting 4 cm² patches into pieces and extracting drug in 50 mL phosphate buffer (pH 7.4) via ultrasonication at 40 °C for 45 minutes (Lab India, Mumbai, India), with shaking every 15 minutes. After cooling, the volume was adjusted to 100 mL, filtered through 0.45 µm membrane, and analyzed at 247 nm using a UV-Vis spectrophotometer (UV-2450, Shimadzu, Mumbai, India). Ten patches per batch were tested, and results were expressed as mg/patch and % theoretical content. Acceptance range was 85–115% with RSD ≤ 5% [36].

Ex Vivo Skin Permeation Studies

Permeation studies were carried out using excised porcine ear skin to assess the effect of novel enhancers and calculate transdermal flux. Fresh skin was collected from a local slaughterhouse, separated from cartilage, stored in phosphate buffer (pH 7.4, 4 °C), and used within 6 hours. Skin integrity was confirmed by measuring electrical resistance (>2 kΩ·cm²). Franz diffusion cells (area: 3.14 cm²) were used with the receptor filled with phosphate buffer containing 20% PEG-400, maintained at 37 ± 1 °C and stirred at 100 rpm. Gel-loaded patches were applied with gentle pressure for 30 seconds. Samples (1 mL) were withdrawn at 0–12 hours and analyzed at 247 nm. Parameters such as lag time, steady-state flux (Jss), permeability coefficient (Kp), and enhancement ratio were calculated. Drug retained in skin was assessed post-study via tape-stripping. Each test was performed in triplicate (n = 3) and analyzed using one-way ANOVA [37].

Moisture Content Analysis

Moisture content in gel-loaded patches was determined using Karl Fischer titration (Metrohm 870 KF Titrino, Mumbai, India). Patch samples (~100 mg) were dissolved in anhydrous methanol and titrated under nitrogen. Results were expressed as % w/w water. Thermogravimetric analysis (TGA 4000, PerkinElmer, Mumbai, India) was also performed on 5–10 mg samples heated from 25–200 °C at 10 °C/min under nitrogen to assess moisture loss. Both tests were conducted in triplicate (n = 3), and findings helped optimize packaging and storage conditions [38].

Stability Studies

Accelerated stability studies were conducted per ICH guidelines to assess patch shelf-life. Patches were sealed in aluminum pouches with desiccant and stored at 40 ± 2 °C/75 ± 5% RH (Thermolab, Mumbai, India) for 6 months; control samples were kept at 25 ± 2 °C/60 ± 5% RH. Samples were withdrawn at 0, 1, 2, 3, and 6 months for evaluation of physical appearance, seal integrity, drug content, adhesion, and in vitro drug release. Observations included color change, delamination, and leakage, with data used to confirm product stability [39].

In Vivo Rheumatoid Arthritis Activity

Experimental Animals

Male Wistar rats (180–220 g) were obtained from the Central Animal House, AIIMS, New Delhi, and housed under standard conditions (25 ± 2 °C, 60 ± 5% RH, 12 h light/dark cycle) with free access to food (Hindustan Lever Ltd., Mumbai, India) and water. Animals were acclimatized for 7 days before the study. The protocol was approved by IAEC (Protocol No. IAEC/2024/RA-021) as per CPCSEA guidelines. Sample size (n=6/group) was calculated using G*Power 3.1.9.7 ($\alpha = 0.05$, power = 0.80, effect size = 1.2), and rats were randomly assigned to groups using computer-generated sequences. Animal welfare was ensured throughout the experiment [40].

Complete Freund's Adjuvant-Induced Arthritis Model

Rheumatoid arthritis was induced by intradermal injection of 0.1 mL CFA (10 mg/mL Mycobacterium tuberculosis H37Ra in mineral oil; Difco, Mumbai, India) at the tail base under light isoflurane anesthesia. Post-injection, animals were monitored and housed individually. Arthritis signs developed by

day 7 and peaked between days 12–16, mimicking human RA. The study continued for 28 days. Arthritis severity was assessed using clinical scoring, paw volume via digital plethysmometer (UGO Basile, Italy), and body weight monitoring. Blood samples (0.5 mL) were collected on days 0, 14, and 28 for hematological and biochemical analysis. Animals in distress or with >20% weight loss were euthanized. At the study end, rats were sacrificed via CO_2 asphyxiation, and joint tissues were collected for histopathology and inflammatory marker evaluation [41].

Table 4: Experimental Group Classification for Anti-Arthritic Activity Assessment

Group	Treatment	Dose/Application	Route	Animals (n)
Group I	Normal Control	-	-	6
Group II	Arthritic Control (CFA)	0.1 mL	Intradermal	6
Group III	Standard Treatment	Diclofenac gel (1% w/w)	Topical	6
Group IV	Optimized Patch (GT3)	Baricitinib (1 mg)	Transdermal	6
Group V	Control Patch	Placebo patch	Transdermal	6

RESULTS AND DISCUSSION

RESULTS

The calibration curve of baricitinib in methanol exhibited excellent linearity over the concentration range of 5–30 µg/mL with a correlation coefficient (R^2) of 0.9998, indicating high precision and reliability of the analytical method. The linear regression equation was found to be $y = 0.0242x + 0.0035$, demonstrating a strong direct relationship between absorbance and concentration (Figure 1).

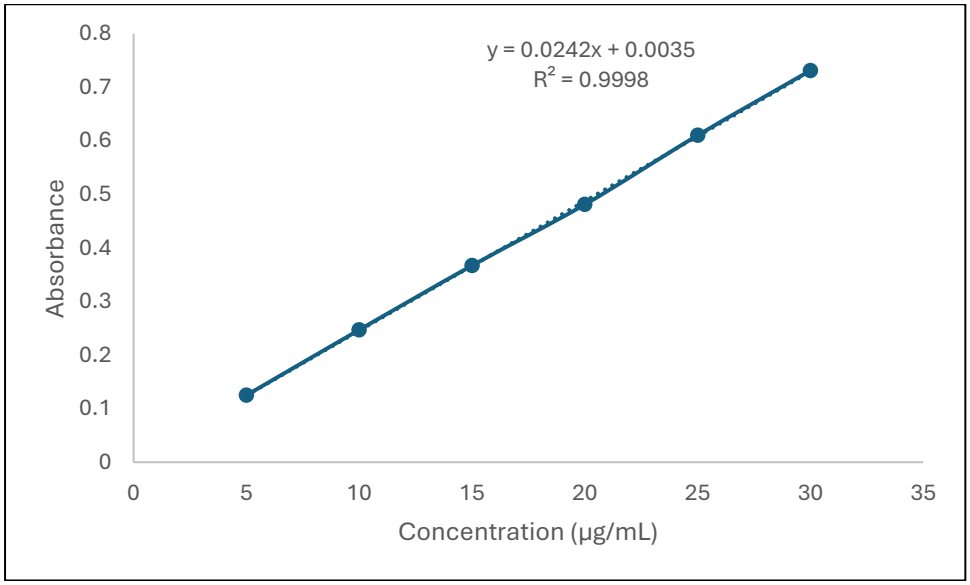

Figure 1: Calibration Curve of Baricitinib in Methanol

Solubility study

Baricitinib exhibited highest solubility in DMSO (74.0 ± 1.0 mg/mL), categorizing it as freely soluble, followed by methanol (21.4 ± 0.6 mg/mL), where it was sparingly soluble. In contrast, its solubility was very slightly soluble in ethanol (0.40 ± 0.05 mg/mL), phosphate buffer pH 6.8 (0.46 ± 0.04 mg/mL), and distilled water (0.36 ± 0.03 mg/mL), indicating the need for solubilizers or enhancers in aqueous formulations (Table 5).

Table 5: Results of solubility study

Solvent	Mean ± SD (mg/mL)	Inferred Solubility Class
DMSO	74.0 ± 1.0	Freely Soluble
Methanol	21.4 ± 0.6	Sparingly Soluble
Ethanol	0.40 ± 0.05	Very Slightly Soluble
Phosphate Buffer (pH 6.8)	0.46 ± 0.04	Very Slightly Soluble
Distilled Water	0.36 ± 0.03	Very Slightly Soluble

All values are expressed as mean±SD

Differential scanning calorimetry

Differential scanning calorimetry (DSC) thermograms showed a sharp endothermic peak for pure baricitinib at 214.94 °C, indicating its crystalline nature. The physical mixture displayed similar peaks at 107.88 °C and 216.15 °C without significant shift or disappearance, suggesting absence of any major interaction between baricitinib and excipients. These findings confirm thermal stability and compatibility of the drug with formulation components (Figure 2).

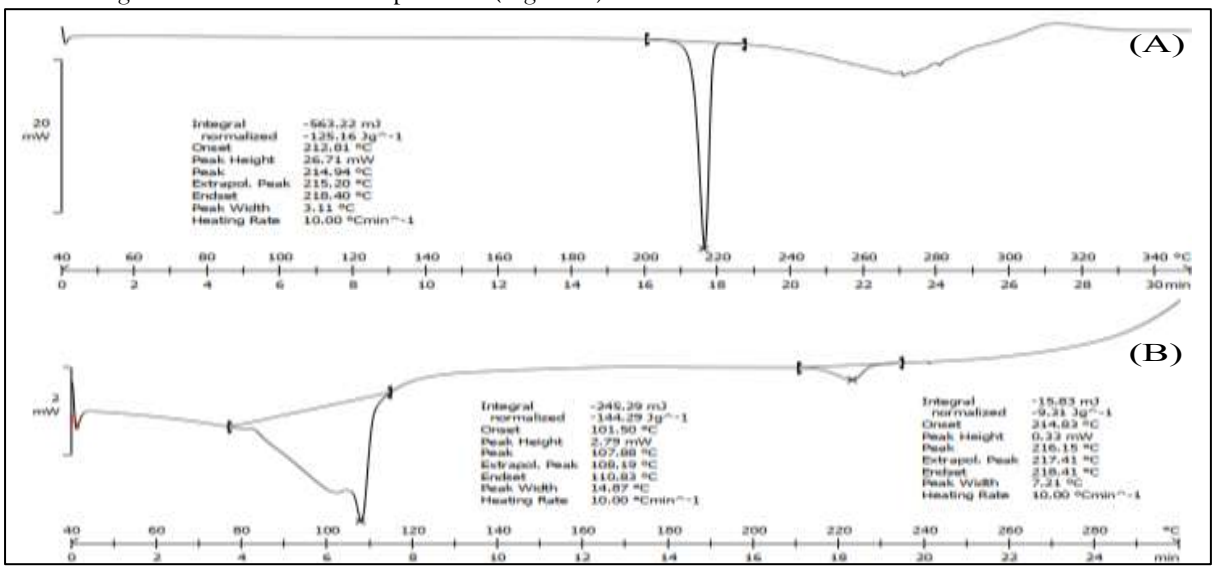

Figure 2: DSC spectra of (A) Pure baricitinib (214.94 °C) (B) Physical mixture (107.88 and 216.15 °C)

FTIR analysis

The FTIR analysis revealed characteristic peaks for pure baricitinib at 3539.7 cm^{-1} (O–H/N–H stretching), 2974.69 cm^{-1} (C–H stretching), and 1655.59 cm^{-1} (C=O stretching), indicating its structural integrity. The physical mixture (Figure 3B) exhibited all major peaks of baricitinib without significant shifting or disappearance, suggesting no chemical interaction between the drug and excipients. Thus, FTIR spectra confirmed compatibility and the absence of potential incompatibilities (Figure 3).

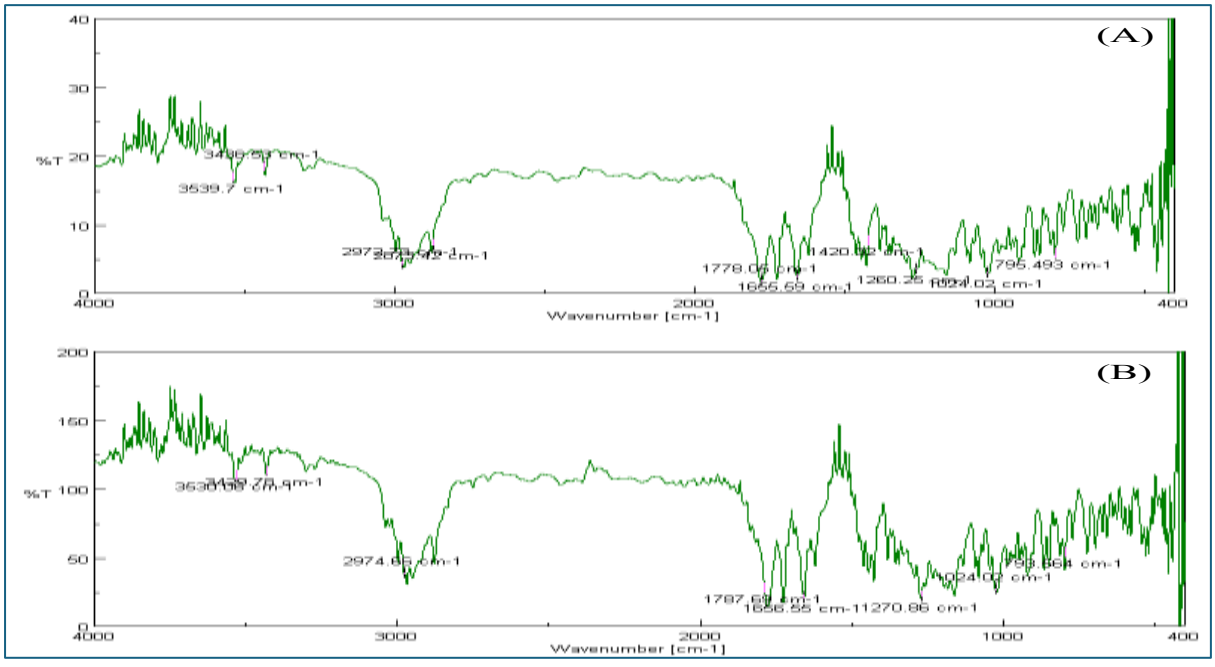

Figure 3: FTIR spectra of (A) Pure drug (B) physical mixture

Evaluations of Baricitinib Gel

All gel formulations exhibited acceptable physicochemical characteristics with pH values ranging from 6.7 to 6.9, suitable for topical application. Viscosity increased proportionally from F1 (1245 ± 65 cP) to F9 (3789 ± 165 cP), correlating with polymer concentration. Spreadability decreased with rising viscosity, from 4.2 ± 0.18 cm (F1) to 1.6 ± 0.09 cm (F9), indicating inverse relation. Drug content remained consistently high across batches (97.6–99.5%), ensuring uniformity. Gel strength increased from 145 ± 8 g (F1) to 312 ± 16 g (F9), confirming formulation robustness (Table 6).

Table 6: Physicochemical Properties of Baricitinib Gel Formulations

Formulation	pH	Viscosity (cP)	Spreadability (cm)	Drug Content (%)	Gel Strength (g)
F1	6.8 ± 0.12	1245 ± 65	4.2 ± 0.18	97.8 ± 1.2	145 ± 8
F2	6.9 ± 0.08	1568 ± 78	3.9 ± 0.15	98.5 ± 0.9	162 ± 12
F3	6.7 ± 0.15	1892 ± 89	3.6 ± 0.22	99.2 ± 1.1	178 ± 10
F4	6.8 ± 0.09	2156 ± 95	3.1 ± 0.14	97.6 ± 1.4	198 ± 15
F5	6.9 ± 0.11	2478 ± 112	2.8 ± 0.19	98.9 ± 0.8	215 ± 11
F6	6.8 ± 0.14	2789 ± 125	2.5 ± 0.16	99.5 ± 1.0	234 ± 13
F7	6.7 ± 0.10	3145 ± 142	2.1 ± 0.12	98.2 ± 1.3	267 ± 18
F8	6.8 ± 0.13	3456 ± 158	1.9 ± 0.11	99.1 ± 0.7	285 ± 14
F9	6.9 ± 0.12	3789 ± 165	1.6 ± 0.09	98.8 ± 1.1	312 ± 16

Values represent mean ± SD (n=3)

The in vitro drug release profile demonstrated a sustained and formulation-dependent release pattern of baricitinib over 12 hours. Among all formulations, F1 exhibited the highest cumulative release (94.8 ± 3.0%), followed by F2 (89.7 ± 2.8%) and F3 (84.9 ± 2.6%), whereas F9 showed the slowest release (55.2 ± 1.6%). A clear inverse relationship was observed between polymer concentration and drug release rate, indicating that higher Carbopol 940P content retarded drug diffusion through the gel matrix. These release trends are visually represented in Figure 4.

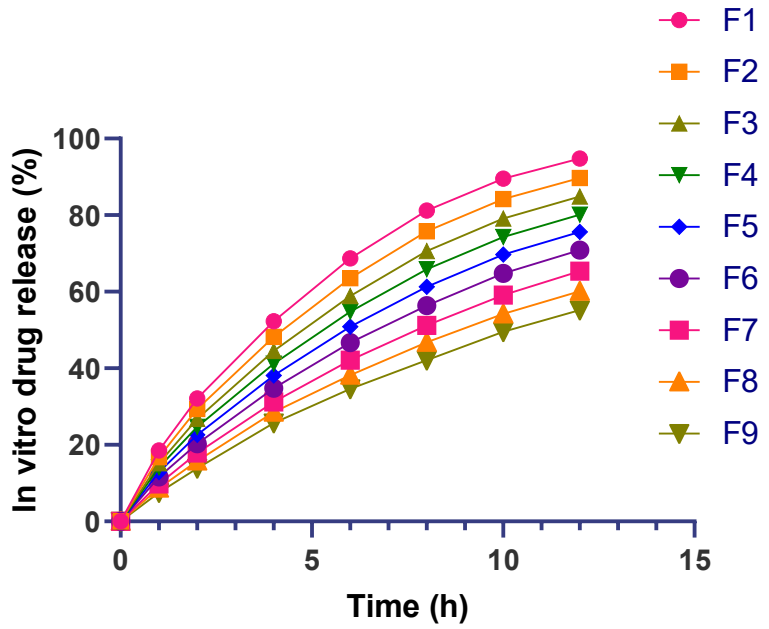

Figure 4: In Vitro Drug Release Profile of Gel formulation

Optimization of Baricitinib gel

Viscosity (Y_1)

The quadratic model applied for the response variable *viscosity* was found to be highly significant, as indicated by the ANOVA results in Table 8. The model showed an extremely high F-value of 24,842.09 and a p-value < 0.0001, confirming model reliability. Among the individual factors, *Carbopol 940P (A)* emerged as the most influential, with an F-value of 111,400.76 and p < 0.0001, followed by *Propylene*

Glycol (B) with an F-value of 12,757.41 and $p < 0.0001$. The quadratic effect of A^2 was also significant ($F = 71.22$, $p = 0.0035$), whereas the interaction term AB and the quadratic term B^2 were statistically insignificant ($p > 0.05$). Fit statistics (Table 7) further validated model strength with $R^2 = 1.0000$, adjusted $R^2 = 0.9999$, and predicted $R^2 = 0.9998$, indicating excellent agreement between observed and predicted values. The low standard deviation (6.95) and coefficient of variation (0.2779%) suggest high precision and reproducibility of the model.

Regression equation for Viscosity (Y_1):

Viscosity (Y_1) = $+2502.00 + 519.78A + 196.74B - 0.75AB + 33.85A^2 - 1.41B^2$

The regression equation indicates that both A (Carbopol 940P) and B (Propylene Glycol) contribute positively to viscosity, with a dominant linear effect of Carbopol. The quadratic term A^2 further enhances viscosity, implying a non-linear relationship. As illustrated in the contour and response surface plots (Figure 5A and 5B), increasing Carbopol concentration resulted in a sharp rise in viscosity, whereas the influence of Propylene Glycol was moderate and more linear. The response surface plot shows a steep curvature along the Carbopol axis, confirming its strong contribution. The contour lines are closely spaced in the direction of Carbopol concentration, supporting a sensitive response to changes in polymer content. The negligible curvature and interaction effects affirm the dominant linear and quadratic influence of Carbopol on viscosity.

Drug Release at 12 Hours (Y_2)

The quadratic model for *drug release at 12 hours* was statistically significant with an F-value of 5160.03 and a p-value < 0.0001 (Table 8). Both main factors *Carbopol 940P (A)* and *Propylene Glycol (B)* showed strong individual effects with F-values of 9304.76 and 1015.30, respectively, and p-values < 0.0001. No interaction or quadratic terms were included due to model optimization favoring a simpler linear form. Fit statistics (Table 7) confirmed the robustness of the model with $R^2 = 0.9994$, adjusted $R^2 = 0.9992$, and predicted $R^2 = 0.9988$. The low standard deviation (0.3754) and coefficient of variation (0.4993%) further supported the accuracy and consistency of the model. Adequate precision (181.47) also exceeded the desirable threshold, ensuring adequate signal-to-noise ratio for prediction.

Regression equation for Drug Release at 12h (Y_2):

Drug Release (Y_2) = $+75.19 - 14.78A - 4.88B$

The negative coefficients for both A and B in the regression equation indicate an inverse relationship with drug release. Increasing Carbopol concentration significantly reduced release due to higher viscosity and gel strength, which likely hindered diffusion. Similarly, a moderate decrease in release was observed with increased Propylene Glycol, potentially due to altered matrix hydration. As evident in the response surface and contour plots (Figure 5C and 5D), maximum drug release was observed at lower levels of both Carbopol and Propylene Glycol. The contour plot revealed elliptical contours, with wider spacing along the B-axis, indicating a stronger suppressive effect of Carbopol compared to Propylene Glycol. The response surface plot showed a declining plane, confirming the negative linear trend and highlighting regions for optimal release profiles.

Table 7: Fit summary of viscosity and drug release at 12 hr.

Response	Source	Sequential p-value	Adjusted R^2	Predicted R^2	
Viscosity	Quadratic	0.0081	0.9999	0.9998	Suggested
Drug release at 12 hr	Linear	< 0.0001	0.9992	0.9988	Suggested

Table 8: ANOVA Summary for Quadratic Models of Viscosity (Y_1) and Drug Release at 12 Hours (Y_2)

Source	Sum of Squares	df	Mean Square	F-value	p-value	
Viscosity						
Model	6.007E+06	5	1.201E+06	24842.09	< 0.0001	significant
A-Carbopol 940P	5.387E+06	1	5.387E+06	1.114E+05	< 0.0001	significant
B-Propylene Glycol	6.170E+05	1	6.170E+05	12757.41	< 0.0001	significant
AB	2.25	1	2.25	0.0465	0.8431	Not significant
A^2	3444.50	1	3444.50	71.22	0.0035	significant
B^2	8.00	1	8.00	0.1654	0.7115	Not significant
Residual	145.08	3	48.36			
Cor Total	6.007E+06	8				
Drug Release at 12h						

Model	1454.36	2	727.18	5160.03	< 0.0001	significant
A-Carbopol 940P	1311.28	1	1311.28	9304.76	< 0.0001	significant
B-Propylene Glycol	143.08	1	143.08	1015.30	< 0.0001	significant
Residual	0.8456	6	0.1409			
Cor Total	1455.21	8				

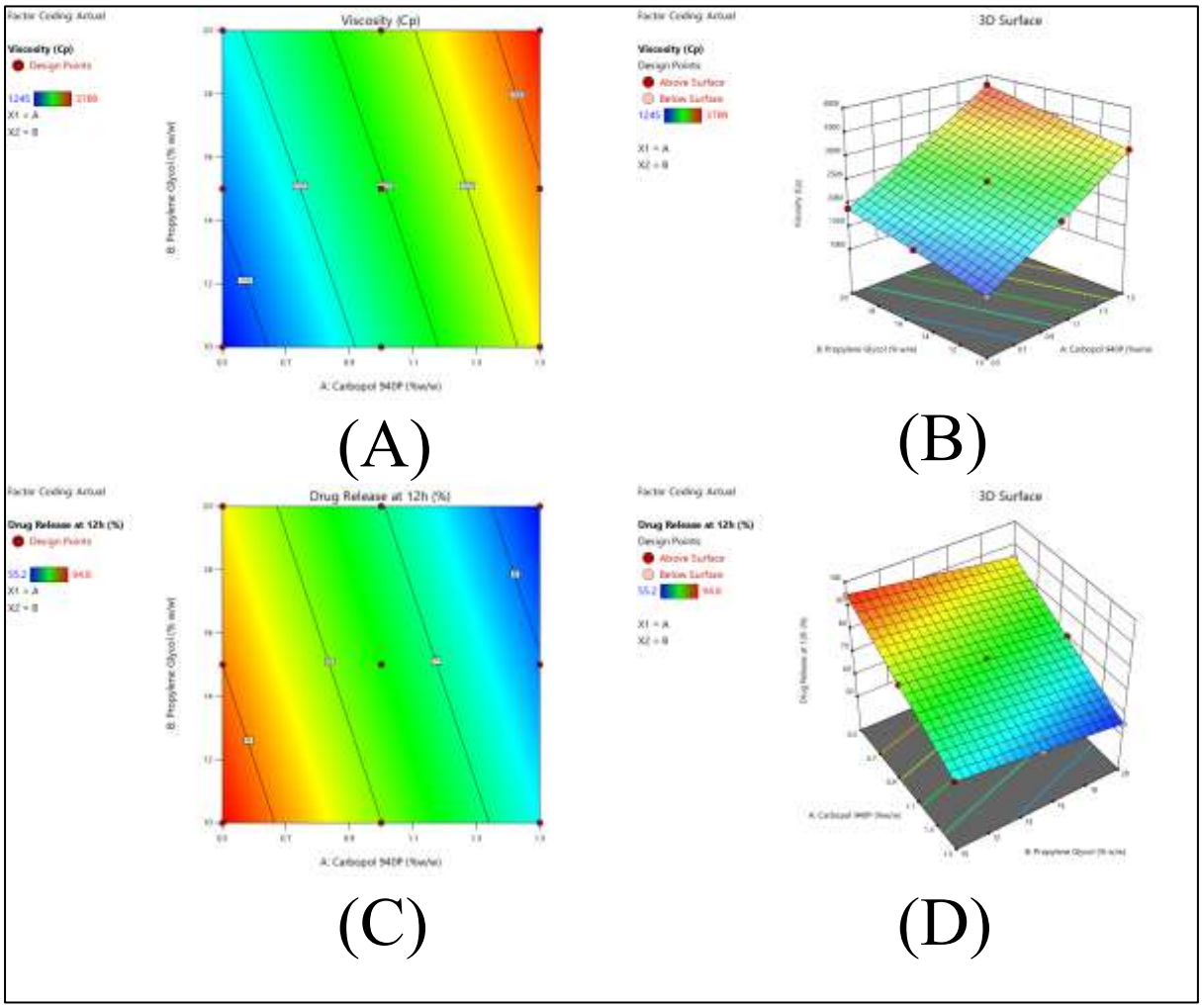

Figure 5: Contour and 3D Surface Plots for Response Variables (A) Contour plot of viscosity (Y_1) as a function of Carbopol 940P (% w/w) and Propylene Glycol (% w/w); (B) 3D surface plot of viscosity (Y_1) showing the effect of formulation variables; (C) Contour plot of drug release at 12 hours (Y_2) in relation to Carbopol 940P and Propylene Glycol concentrations; (D) 3D surface plot illustrating drug release at 12 hours (Y_2) as influenced by formulation factors.

Characterization of gel loaded Transdermal patch

The physicochemical and mechanical evaluation of gel-loaded transdermal patches (GT1–GT4) revealed uniformity across parameters with increasing polymer content. Thickness ranged from 0.24 ± 0.012 mm (GT1) to 0.38 ± 0.021 mm (GT4), while weight increased accordingly. Folding endurance values exceeded 300 folds, with GT4 exhibiting highest flexibility (498 ± 28). Adhesion strength improved progressively, reaching 1.12 ± 0.07 N/cm² in GT4. Drug content remained within acceptable limits (97.2–101.2%), and moisture content decreased with increasing polymer concentration, suggesting improved patch integrity (Table 9).

Table 9: Physicochemical and Mechanical Characterization of Optimized Gel-Loaded Transdermal Patches

Parameter	GT1	GT2	GT3	GT4
Thickness (mm)	0.24 ± 0.012	0.29 ± 0.015	0.33 ± 0.018	0.38 ± 0.021
Weight (mg/4cm²)	185.4 ± 8.2	224.7 ± 9.6	268.3 ± 11.1	315.8 ± 12.4
Folding Endurance	312 ± 18	387 ± 22	445 ± 25	498 ± 28

Adhesion Strength (N/cm²)	0.68 ± 0.04	0.82 ± 0.05	0.94 ± 0.06	1.12 ± 0.07
Drug Content (mg/patch)	0.97 ± 0.03	0.99 ± 0.02	1.01 ± 0.04	0.98 ± 0.03
Drug Content (%)	97.2 ± 3.1	99.1 ± 2.4	101.2 ± 3.8	98.4 ± 2.9
Moisture Content (%)	4.8 ± 0.3	4.2 ± 0.2	3.9 ± 0.3	3.5 ± 0.2

Values represent mean ± SD (n=3)

The visual inspection of transdermal patches (GT1–GT4) showed that all formulations were uniform with no visible defects. GT1 and GT2 exhibited pale yellow color and semi-transparent appearance with excellent surface smoothness, while GT3 and GT4 appeared light yellow and translucent with slightly reduced smoothness. All patches maintained consistent uniformity and acceptable aesthetic quality, confirming good formulation integrity (Table 10).

Table 10: Physical Appearance and Visual Quality Assessment of Transdermal Patch Formulations

Evaluation Parameter	GT1	GT2	GT3	GT4
Color	Pale yellow	Pale yellow	Light yellow	Light yellow
Transparency	Semi-transparent	Semi-transparent	Translucent	Translucent
Surface Smoothness	Excellent	Excellent	Good	Good
Uniformity	Uniform	Uniform	Uniform	Uniform

Transdermal Permeation Kinetics Across Porcine Skin Barrier

The in vitro drug release profile of gel-loaded transdermal patches (GT1–GT4) demonstrated a sustained release pattern over 12 hours. GT1 exhibited the highest cumulative drug release (85.2 ± 3.4%), followed by GT2 (75.8 ± 3.1%), GT3 (66.9 ± 2.8%), and GT4 (57.4 ± 2.5%). A direct correlation between formulation composition and release rate was observed, indicating the influence of gel viscosity and patch thickness on diffusion. The release kinetics are visually represented in Figure 6.

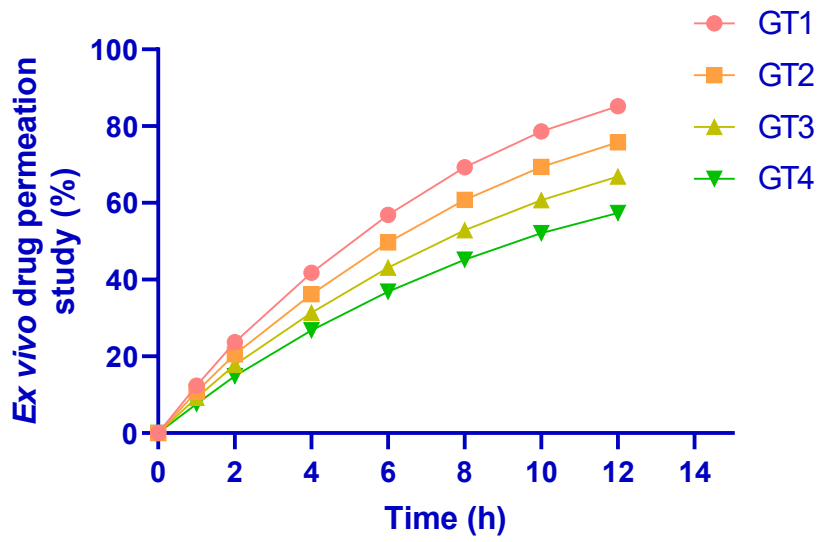

Figure 6: Ex Vivo Skin Permeation study for gel loaded patch

Formulation GT1 exhibited superior permeation performance with the lowest lag time (0.42 ± 0.08 h), highest steady-state flux (28.4 ± 1.6 µg/cm²/h), and highest permeability coefficient (2.84 ± 0.16 × 10^{-3} cm/h), followed by GT2, GT3, and GT4. Correspondingly, the enhancement ratio decreased from 4.73 to 3.03 across the formulations. Conversely, skin retention increased with higher formulation viscosity, peaking at 26.2 ± 1.9 µg/cm² for GT4, as depicted in Table 11.

Table 11: Permeation Enhancement and Pharmacokinetic Parameters

Parameter	GT1	GT2	GT3	GT4
Lag Time (h)	0.42 ± 0.08	0.58 ± 0.12	0.74 ± 0.15	0.91 ± 0.18
Steady State Flux (µg/cm²/h)	28.4 ± 1.6	24.8 ± 1.4	21.5 ± 1.2	18.2 ± 1.0
Permeability Coefficient (cm/h × 10^{-3})	2.84 ± 0.16	2.48 ± 0.14	2.15 ± 0.12	1.82 ± 0.10
Enhancement Ratio*	4.73 ± 0.28	4.13 ± 0.24	3.58 ± 0.21	3.03 ± 0.18

Skin Retention (μg/cm²)	18.6 ± 1.2	21.4 ± 1.5	23.8 ± 1.7	26.2 ± 1.9

The accelerated stability study of the optimized GT3 patch over six months at 40 ± 2 °C/75 ± 5% RH showed minimal changes in key attributes (Table 12). Drug content slightly decreased from 101.2 ± 3.8% initially to 97.4 ± 3.6% at 6 months, remaining within acceptable limits. Adhesion strength showed a gradual decline from 0.94 ± 0.06 N/cm² to 0.82 ± 0.08 N/cm², while folding endurance reduced from 445 ± 25 to 418 ± 35. Moisture content consistently dropped from 3.9 ± 0.3% to 3.1 ± 0.3%.

Table 12: Accelerated Stability Performance of Optimized Transdermal Patch (GT3)

Parameter	Initial	1 Month	2 Months	3 Months	6 Months
Drug Content (%)	101.2 ± 3.8	100.7 ± 3.2	99.8 ± 3.5	98.9 ± 3.1	97.4 ± 3.6
Adhesion Strength (N/cm²)	0.94 ± 0.06	0.92 ± 0.05	0.89 ± 0.07	0.86 ± 0.06	0.82 ± 0.08
Drug Release at 8h (%)	52.9 ± 2.2	53.4 ± 2.4	54.1 ± 2.6	54.8 ± 2.8	55.6 ± 3.1
Moisture Content (%)	3.9 ± 0.3	3.7 ± 0.2	3.5 ± 0.3	3.3 ± 0.2	3.1 ± 0.3
Physical Appearance	Normal	Normal	Normal	Normal	Acceptable
Thickness (mm)	0.33 ± 0.018	0.33 ± 0.019	0.32 ± 0.020	0.32 ± 0.021	0.31 ± 0.022
Folding Endurance	445 ± 25	441 ± 28	436 ± 31	429 ± 33	418 ± 35

Storage conditions: 40±2°C/75±5% RH Values represent mean ± SD (n=3)

In Vivo Rheumatoid Arthritis Activity

The in vivo evaluation of rheumatoid arthritis activity demonstrated that the optimized patch (GT3) significantly reduced disease severity across multiple parameters. Clinical arthritis scores (Table 13) showed progressive inflammation in the arthritic control group, reaching 14.2 ± 2.1 by day 28, while GT3 reduced the score to 7.2 ± 1.2, comparable to the standard treatment (8.4 ± 1.5). GT3 was superior to the control patch, which reached 13.6 ± 2.3. Similarly, GT3 effectively limited paw swelling, with final paw volume at 2.26 ± 0.19 mL and 60.8% inhibition greater than the standard group's 53.4% (Table 14).

Table 13: Clinical Arthritis Scoring and Joint Assessment Parameters

Parameter	Day 0	Day 7	Day 14	Day 21	Day 28
Normal Control	0.0 ± 0.0	0.0 ± 0.0	0.0 ± 0.0	0.0 ± 0.0	0.0 ± 0.0
Arthritic Control	0.0 ± 0.0	2.8 ± 0.4	8.6 ± 1.2	12.4 ± 1.8	14.2 ± 2.1
Standard Treatment	0.0 ± 0.0	2.6 ± 0.5	6.2 ± 1.0	7.8 ± 1.3	8.4 ± 1.5
Optimized Patch (GT3)	0.0 ± 0.0	2.7 ± 0.3	5.8 ± 0.9	6.9 ± 1.1	7.2 ± 1.2
Control Patch	0.0 ± 0.0	2.9 ± 0.6	8.1 ± 1.4	11.8 ± 1.9	13.6 ± 2.3

Arthritis scoring: 0=normal, 1=mild swelling, 2=moderate swelling, 3=severe swelling, 4=maximum swelling with joint rigidity Values represent mean ± SD (n=6)

Table 14: Paw Volume Changes and Anti-Inflammatory Assessment

Treatment Group	Day 0	Day 7	Day 14	Day 21	Day 28	% Inhibition*
Normal Control	1.42 ± 0.08	1.44 ± 0.07	1.45 ± 0.09	1.46 ± 0.08	1.47 ± 0.09	-
Arthritic Control	1.41 ± 0.09	1.98 ± 0.15	2.86 ± 0.21	3.24 ± 0.28	3.58 ± 0.32	-
Standard Treatment	1.43 ± 0.07	1.89 ± 0.12	2.15 ± 0.18	2.31 ± 0.19	2.42 ± 0.22	53.4
Optimized Patch (GT3)	1.42 ± 0.08	1.85 ± 0.11	2.08 ± 0.16	2.18 ± 0.17	2.26 ± 0.19	60.8
Control Patch	1.44 ± 0.09	1.96 ± 0.14	2.79 ± 0.23	3.18 ± 0.26	3.51 ± 0.31	3.2

Paw volume measured in mL using digital plethysmometer % Inhibition calculated relative to arthritic control on day 28 Values represent mean ± SD (n=6)

Body weight loss observed in the arthritic control group (−13.4%) was mitigated by GT3 (+1.7%), suggesting improved general health maintenance (Table 15). Hematological parameters (Table 16) further confirmed GT3's therapeutic efficacy, with significant recovery in hemoglobin (13.1 ± 0.7 g/dL), RBC

count (7.1 ± 0.4 ×10^6/μL), and normalization of WBC and ESR compared to the untreated group ($p<0.05$). Inflammatory biomarkers and cytokines (Table 17) also showed marked suppression in GT3-treated rats—TNF-α, IL-1β, IL-6, CRP, and RF levels were all significantly lower than the arthritic control, indicating potent anti-inflammatory activity. These findings support the clinical potential of GT3 in rheumatoid arthritis management.

Table 15: Body Weight Changes and General Health Parameters

Treatment Group	Initial Weight (g)	Day 14 (g)	Day 28 (g)	Weight Change (%)
Normal Control	198.4 ± 8.2	215.6 ± 9.1	234.8 ± 10.5	+18.3
Arthritic Control	201.2 ± 9.1	185.7 ± 8.9	174.3 ± 9.8	-13.4
Standard Treatment	199.8 ± 7.8	195.4 ± 8.6	198.9 ± 9.2	-0.5
Optimized Patch (GT3)	202.1 ± 8.4	198.7 ± 8.1	205.6 ± 9.4	+1.7
Control Patch	200.5 ± 8.9	187.2 ± 9.3	176.8 ± 10.2	-11.8

Values represent mean ± SD (n=6)

Table 16: Hematological Parameters in CFA-Induced Arthritic Rats

Parameter	Normal Control	Arthritic Control	Standard Treatment	Optimized Patch	Control Patch
Hemoglobin (g/dL)	14.2 ± 0.8	10.1 ± 1.2*	12.8 ± 0.9#	13.1 ± 0.7#	10.4 ± 1.1*
RBC (×10^6/μL)	7.8 ± 0.4	5.2 ± 0.6*	6.9 ± 0.5#	7.1 ± 0.4#	5.4 ± 0.7*
WBC (×10^3/μL)	8.4 ± 0.6	15.6 ± 1.8*	10.2 ± 1.1#	9.8 ± 0.9#	14.9 ± 1.7*
ESR (mm/1st hr)	12.1 ± 1.2	42.8 ± 3.6*	22.4 ± 2.8#	19.7 ± 2.3#	40.2 ± 3.9*
Platelet Count (×10^3/μL)	456 ± 28	798 ± 52*	589 ± 41#	542 ± 36#	776 ± 48*

Data represents mean ± SD (n=6) $p<0.05$ vs Normal Control; #$p<0.05$ vs Arthritic Control

Table 17: Inflammatory Biomarkers and Cytokine Profile

Biomarker	Normal Control	Arthritic Control	Standard Treatment	Optimized Patch	Control Patch
TNF-α (pg/mL)	28.4 ± 3.2	156.8 ± 18.5*	78.9 ± 8.9#	64.2 ± 7.1#	148.6 ± 16.8*
IL-1β (pg/mL)	15.2 ± 2.1	89.6 ± 11.4*	48.7 ± 6.2#	42.1 ± 5.8#	85.3 ± 10.9*
IL-6 (pg/mL)	22.1 ± 2.8	124.7 ± 15.2*	68.4 ± 8.1#	58.9 ± 6.9#	119.2 ± 14.6*
CRP (mg/L)	2.1 ± 0.4	18.6 ± 2.3*	8.9 ± 1.2#	7.2 ± 1.0#	17.4 ± 2.1*
RF (IU/mL)	8.4 ± 1.1	45.7 ± 5.8*	24.1 ± 3.2#	19.8 ± 2.6#	43.2 ± 5.4*

Data represents mean ± SD (n=6) $p<0.05$ vs Normal Control; #$p<0.05$ vs Arthritic Control

DISCUSSION

The present study successfully formulated and optimized a Baricitinib-loaded transdermal gel-patch system intended for enhanced rheumatoid arthritis therapy. The solubility studies (Table 5) revealed that Baricitinib exhibited maximum solubility in DMSO (74.0 ± 1.0 mg/mL), followed by methanol (21.4 ± 0.6 mg/mL), suggesting DMSO as a suitable co-solvent for ensuring drug loading and uniform dispersion within the polymeric gel matrix. The calibration curve of Baricitinib in methanol (Figure 1) demonstrated linearity with excellent correlation ($R^2 > 0.99$), confirming the reliability of the UV spectrophotometric method used for drug content and release studies [42]. Preformulation compatibility was confirmed by FTIR (Figure 3) and DSC studies (Figure 2). The FTIR spectra exhibited preservation of characteristic peaks of Baricitinib in the physical mixture, indicating no chemical interaction with excipients. DSC thermograms revealed a sharp melting peak for pure Baricitinib at 214.94 °C, and a slightly shifted peak at 216.15 °C in the physical mixture, which suggests no significant interaction or loss of drug crystallinity [43]. The gel formulations F1–F9 were evaluated for critical quality attributes (Table 6), where F9 exhibited the highest viscosity (3789 ± 165 cP), lowest spreadability (1.6 ± 0.09 cm), and high

drug content (98.8 ± 1.1%). These trends reflected the concentration-dependent influence of Carbopol 940P on gel consistency and mechanical integrity [44].

The in vitro drug release profiles over 12 hours (Figure 4, Table data) showed a sustained release pattern across formulations, with F1 exhibiting the fastest release (94.8 ± 3.0%) and F9 the slowest (55.2 ± 1.6%), affirming the inverse relationship between polymer concentration and drug diffusion [45]. The optimized transdermal patches (GT1–GT4) displayed progressive increases in patch thickness, weight, folding endurance, and adhesion strength with increasing gel load (Table 9). GT3 demonstrated an ideal balance between mechanical strength (445 ± 25), adhesion (0.94 ± 0.06 N/cm²), and drug content (101.2 ± 3.8%), qualifying it for further in vitro and in vivo assessments [46]. Visual assessment of patches (Table 10) confirmed acceptable quality with uniform appearance, translucency, and smooth surface. The in vitro drug release profile of GT1 to GT4 (Figure 6) demonstrated a time-dependent release, with GT1 exhibiting 85.2 ± 3.4% and GT4 the least (57.4 ± 2.5%) after 12 hours. These findings align with the increasing gel matrix density and subsequent diffusion resistance. Ex vivo permeation data (Table 11) revealed that GT1 had the highest steady-state flux (28.4 ± 1.6 μg/cm²/h) and permeability coefficient (2.84×10^{-3} cm/h), while GT4 showed the highest skin retention (26.2 ± 1.9 μg/cm²), confirming the modulation of permeation by gel content [47].

Accelerated stability testing of GT3 over six months (Table 12) demonstrated stable drug content (97.4 ± 3.6%), consistent adhesion strength (0.82 ± 0.08 N/cm²), and improved drug release (55.6 ± 3.1% at 8 h), with no significant changes in physical attributes or moisture content, indicating good shelf stability under stress conditions [48]. In vivo efficacy was evaluated in CFA-induced arthritic rats. Clinical arthritis scoring (Table 13) revealed significant suppression of disease progression in the GT3-treated group compared to the arthritic control, with scores reducing to 7.2 ± 1.2 by Day 28 versus 14.2 ± 2.1 in the control group [49]. GT3 also achieved a 60.8% inhibition of paw edema (Table 14), surpassing the standard treatment group (53.4%). Body weight monitoring (Table 15) showed that GT3-treated animals maintained or slightly increased weight (+1.7%), while arthritic controls lost 13.4%, indicating improved general health. Hematological analysis (Table 16) supported anti-arthritic potential, with GT3 significantly restoring hemoglobin (13.1 ± 0.7 g/dL) and RBC levels ($7.1 \pm 0.4 \times 10^6$/μL) while reducing WBC count ($9.8 \pm 0.9 \times 10^3$/μL), ESR (19.7 ± 2.3 mm/hr), and platelet count ($542 \pm 36 \times 10^3$/μL) compared to the arthritic control. Furthermore, pro-inflammatory cytokine levels (TNF-α, IL-1β, IL-6) and biomarkers (CRP, RF) were significantly suppressed in GT3-treated rats (Table 17), validating its anti-inflammatory and disease-modifying effects comparable to the standard group [50].

Collectively, the results suggest that the GT3 gel-loaded transdermal patch delivers Baricitinib effectively, providing sustained drug release, improved skin retention, excellent mechanical stability, and marked therapeutic benefit in arthritic conditions. The data presented across Figures 1–6 and Tables 5–17 clearly illustrate the comprehensive performance evaluation and potential clinical relevance of this formulation [51].

CONCLUSION

The study successfully developed and optimized a Baricitinib-loaded gel-based transdermal patch (GT3) demonstrating superior physicochemical properties, sustained drug release, enhanced skin permeation, and excellent in vivo anti-arthritic efficacy. The optimized formulation maintained mechanical integrity, stability, and therapeutic consistency over six months. In vivo evaluations in arthritic rats revealed significant suppression of inflammation, restoration of hematological parameters, and downregulation of pro-inflammatory cytokines, comparable to standard treatment. These findings suggest that GT3 offers a promising, non-invasive alternative for long-term management of rheumatoid arthritis with improved patient compliance and reduced systemic side effects. The potential clinical benefits of this transdermal system lie in its controlled delivery, skin-targeted action, and enhanced therapeutic performance. Further advanced pharmacokinetic, safety, and clinical trials are recommended to confirm translational applicability and therapeutic viability in human subjects.

Abbreviations

ANOVA: Analysis of Variance; FTIR: Fourier-transform Infrared Spectroscopy; UV: Ultraviolet Spectroscopy; DSC: Differential Scanning Calorimetry; SD: Standard Deviation; RH: Relative Humidity; HPLC: High Performance Liquid Chromatography; DMSO: Dimethyl Sulfoxide; TNF-α: Tumor Necrosis Factor-alpha; IL-1β: Interleukin-1 beta; IL-6: Interleukin-6; CRP: C-Reactive Protein; RF: Rheumatoid Factor; ESR: Erythrocyte Sedimentation Rate; RBC: Red Blood Cells; WBC: White Blood

Cells; SEM: Standard Error of Mean; C.V.: Coefficient of Variation; n: Number of observations; N: Newton; cm: Centimeter; mm: Millimeter; mL: Milliliter; µg: Microgram; pg: Picogram.

REFERENCES

1. Safiri S, Kolahi AA, Hoy D, Smith E, Bettampadi D, Mansournia MA, et al. Global, regional and national burden of rheumatoid arthritis 1990-2017: a systematic analysis of the Global Burden of Disease study 2017. Ann Rheum Dis. 2019;78(11):1463-71. doi: 10.1136/annrheumdis-2019-215920
2. GBD 2021 Rheumatoid Arthritis Collaborators. Global, regional, and national burden of rheumatoid arthritis, 1990–2020, and projections to 2050: a systematic analysis of the Global Burden of Disease Study 2021. Lancet Rheumatol. 2023;5(10):e594-610. doi: 10.1016/S2665-9913(23)00211-4
3. World Health Organization. Rheumatoid arthritis [Internet]. Geneva: WHO; 2023 [cited 2024 Dec 30]. Available from: https://www.who.int/news-room/fact-sheets/detail/rheumatoid-arthritis
4. Zhang Z, Gao X, Chen W, Li Q, Wang Y, Zhang L. Global, regional and national burden of rheumatoid arthritis from 1990 to 2021, with projections of incidence to 2050: a systematic and comprehensive analysis of the Global Burden of Disease study 2021. Biomark Res. 2025;13(1). doi: 10.1186/s40364-025-00760-8
5. Zhang Z, Gao X. Global, regional, and national epidemiology of rheumatoid arthritis among people aged 20–54 years from 1990 to 2021. Sci Rep. 2025;15:2150. doi: 10.1038/s41598-025-92150-1
6. Mogul A, Corsi K, McAuliffe L. Baricitinib: The Second FDA-Approved JAK Inhibitor for the Treatment of Rheumatoid Arthritis. Ann Pharmacother. 2019;53(9):947-53. doi: 10.1177/1060028019839650
7. Smolen JS, Landewé RBM, Bijlsma JWJ, Burmester GR, Dougados M, Kerschbaumer A, et al. EULAR recommendations for the management of rheumatoid arthritis with synthetic and biological disease-modifying antirheumatic drugs: 2019 update. Ann Rheum Dis. 2020;79(6):685-99. doi: 10.1136/annrheumdis-2019-216655
8. Eli Lilly and Company. FDA Approves OLUMIANT® (baricitinib) 2-mg Tablets for the Treatment of Adults with Moderately-to-Severely Active Rheumatoid Arthritis [Internet]. Indianapolis: Eli Lilly; 2018 [cited 2024 Dec 30]. Available from: https://investor.lilly.com/news-releases/news-release-details/fda-approves-olumiantr-baricitinib-2-mg-tablets-treatment-adults
9. Taylor PC, Keystone EC, van der Heijde D, Weinblatt ME, Del Carmen Morales L, Reyes Gonzaga J, et al. Baricitinib versus placebo or adalimumab in rheumatoid arthritis. N Engl J Med. 2017;376(7):652-62. doi: 10.1056/NEJMoa1608345
10. Genovese MC, Kremer J, Zamani O, Ludivico C, Krogulec M, Xie L, et al. Baricitinib in patients with refractory rheumatoid arthritis. N Engl J Med. 2016;374(13):1243-52. doi: 10.1056/NEJMoa1507247
11. Pastore MN, Kalia YN, Horstmann M, Roberts MS. Transdermal patches: history, development and pharmacology. Br J Pharmacol. 2015;172(9):2179-209. doi: 10.1111/bph.13059
12. Prausnitz MR, Langer R. Transdermal drug delivery. Nat Biotechnol. 2008;26(11):1261-8. doi: 10.1038/nbt.1504
13. Bird S, Lwin Z, Ahmed T. Transdermal drug delivery and patches—An overview. Med Devices Sens. 2020;3(2):e10069. doi: 10.1002/mds3.10069
14. Ita K. Recent advances in transdermal drug delivery systems: a review. Biomater Res. 2021;25(1):20. doi: 10.1186/s40824-021-00226-6
15. Zhang Y, Wang J, Yu J, Wen D, Kahkoska AR, Lu Y, et al. Wearable patches for transdermal drug delivery. Adv Drug Deliv Rev. 2023;194:114724. doi: 10.1016/j.addr.2023.114724
16. International Council for Harmonisation of Technical Requirements for Pharmaceuticals for Human Use. ICH Q2(R1) Validation of analytical procedures: text and methodology [Internet]. Geneva: ICH; 2005 [cited 2024 Dec 30]. Available from: https://database.ich.org/sites/default/files/Q2%28R1%29%20Guideline.pdf
17. Sinko PJ, Singh Y. Martin's Physical Pharmacy and Pharmaceutical Sciences. 6th ed. Philadelphia: Lippincott Williams & Wilkins; 2011.
18. Brittain HG, editor. Polymorphism in Pharmaceutical Solids. 2nd ed. New York: Informa Healthcare; 2009.
19. Pavia DL, Lampman GM, Kriz GS, Vyvyan JR. Introduction to Spectroscopy. 5th ed. Boston: Cengage Learning; 2014.
20. Montgomery DC. Design and Analysis of Experiments. 9th ed. New York: John Wiley & Sons; 2017.
21. Box GE, Hunter WG, Hunter JS. Statistics for Experimenters: An Introduction to Design, Data Analysis, and Model Building. New York: John Wiley & Sons; 1978.
22. Naik A, Kalia YN, Guy RH. Transdermal drug delivery: overcoming the skin's barrier function. Pharm Sci Technolo Today. 2000;3(9):318-26. doi: 10.1016/s1461-5347(00)00295-9
23. Banker GS, Rhodes CT, editors. Modern Pharmaceutics. 4th ed. New York: Marcel Dekker; 2002.
24. United States Pharmacopeia and National Formulary. USP 43-NF 38. Rockville: United States Pharmacopeial Convention; 2020.
25. Malkin AY, Isayev AI. Rheology: Concepts, Methods and Applications. 3rd ed. Toronto: ChemTec Publishing; 2017.
26. Aulton ME, Taylor KM, editors. Aulton's Pharmaceutics: The Design and Manufacture of Medicines. 5th ed. Edinburgh: Elsevier; 2018.
27. British Pharmacopoeia Commission. British Pharmacopoeia 2022. London: The Stationery Office; 2021.
28. Steffe JF. Rheological Methods in Food Process Engineering. 2nd ed. East Lansing: Freeman Press; 1996.
29. Rowe RC, Sheskey PJ, Quinn ME, editors. Handbook of Pharmaceutical Excipients. 6th ed. London: Pharmaceutical Press; 2009.
30. Costa P, Sousa Lobo JM. Modeling and comparison of dissolution profiles. Eur J Pharm Sci. 2001;13(2):123-33. doi: 10.1016/s0928-0987(01)00095-1
31. Gibson M, editor. Pharmaceutical Preformulation and Formulation: A Practical Guide from Candidate Drug Selection to Commercial Dosage Form. 2nd ed. New York: Informa Healthcare; 2009.
32. Swarbrick J, editor. Encyclopedia of Pharmaceutical Technology. 3rd ed. New York: Informa Healthcare; 2007.

33. European Pharmacopoeia Commission. European Pharmacopoeia 10.0. Strasbourg: Council of Europe; 2019.
34. Liberman HA, Rieger MM, Banker GS, editors. Pharmaceutical Dosage Forms: Disperse Systems. 2nd ed. New York: Marcel Dekker; 1996.
35. Minghetti P, Cilurzo F, Montanari L. Evaluation of adhesive properties of patches based on acrylic matrices. Drug Dev Ind Pharm. 1999;25(1):1-6. doi: 10.1081/ddc-100102139
36. Food and Drug Administration. Guidance for Industry: Dissolution Testing of Immediate Release Solid Oral Dosage Forms [Internet]. Rockville: FDA; 1997 [cited 2024 Dec 30]. Available from: https://www.fda.gov/media/70936/download
37. Franz TJ. Percutaneous absorption on the relevance of in vitro data. J Invest Dermatol. 1975;64(3):190-5. doi: 10.1111/1523-1747.ep12533356
38. Karl Fischer titration in pharmaceutical analysis. Pharm Technol. 2008;32(10):72-6.
39. International Council for Harmonisation of Technical Requirements for Pharmaceuticals for Human Use. ICH Q1A(R2) Stability testing of new drug substances and products [Internet]. Geneva: ICH; 2003 [cited 2024 Dec 30]. Available from: https://database.ich.org/sites/default/files/Q1A%28R2%29%20Guideline.pdf
40. Committee for the Update of the Guide for the Care and Use of Laboratory Animals. Guide for the Care and Use of Laboratory Animals. 8th ed. Washington: National Academies Press; 2011.
41. Chondrex Inc. Adjuvant-Induced Arthritis Model [Internet]. Redmond: Chondrex; 2024 [cited 2024 Dec 30]. Available from: https://www.chondrex.com/animal-models/adjuvant-induced-arthritis-adjuvants
42. Abdallah NM, Elsabahy M, Ragab DM, Fathalla D. Enhancing bioavailability and controlling release of glimepiride using various polyethylene glycol solid dispersions. Drug Des Devel Ther. 2015;9:2915-24. doi: 10.2147/DDDT.S83070
43. Giron D. Thermal analysis and calorimetric methods in the characterisation of polymorphs and solvates. Thermochim Acta. 1995;248:1-59. doi: 10.1016/0040-6031(94)01953-E
44. Rowe RC, Sheskey PJ, Cook WG, Quinn ME, editors. Handbook of Pharmaceutical Excipients. 7th ed. London: Pharmaceutical Press; 2012.
45. Siepmann J, Peppas NA. Higuchi equation: derivation, applications, use and misuse. Int J Pharm. 2011;418(1):6-12. doi: 10.1016/j.ijpharm.2011.03.051
46. Chien YW. Transdermal Drug Delivery and Delivery Systems. In: Swarbrick J, Boylan JC, editors. Encyclopedia of Pharmaceutical Technology. New York: Marcel Dekker; 1995. p. 299-321.
47. Kalia YN, Guy RH. Modeling transdermal drug release. Adv Drug Deliv Rev. 2001;48(2-3):159-72. doi: 10.1016/s0169-409x(01)00113-2
48. Watkinson AC, Kearney MC, Quinn HL, Courtenay AJ, Donnelly RF. Future of the transdermal drug delivery market. Ther Deliv. 2016;7(4):249-73. doi: 10.4155/tde.16.6
49. Pearson CM. Development of arthritis, periarthritis and periostitis in rats given adjuvants. Proc Soc Exp Biol Med. 1956;91(1):95-101. doi: 10.3181/00379727-91-22179
50. Bendele A. Animal models of rheumatoid arthritis. J Musculoskelet Neuronal Interact. 2001;1(4):377-85.
51. Taneja A, Bhat M, Arora S. Rheumatoid arthritis: pathophysiology and modern drug therapy. J Crit Rev. 2018;5(2):1-10. doi: 10.22159/jcr.2018v5i2.25313
52. Chaudhary, Pankaj Haribhau and Kandalkar, Ashish and Jawarkar, Somkant and Dhole, Rakesh and Tiwari, Vinod and Chachda, Nilesh and Patil, Neha and Darekar, Geeta, Exploring the Influence of Permeation Enhancer (Cinnamon Bark Extracts) on the Bioavailability of Fenofibrate Formulated Transdermal Patches (December 10, 2023). Eur. Chem. Bull. 2023; 12 (8): 9215-9223
53. Kandalkar A, Chachda N, Jawarkar S, Patel A, Wagh H, Gore S, Kulkarni S, Dhole R. Formulation And Development Of Transdermal Patches Of Amoxicillin And Comparative Effect Of Natural Permeation Enhancers On Ex Vivo Release. Journal of Namibian Studies. 2023 Jan 7;33.
54. Darji P, Patel J, Patel R, Patel B, Khatri V, Fnu PI, Nalla S. SELF-REGULATED ANTI-OVERDOSE CRUSH-RESISTANT DRUG DELIVERY SYSTEM DESIGNED TO ADDRESS THE OPIOID ABUSE CRISIS. World journal of pharmaceutical research. 2024 Apr 2;13(10):997-1014.